Proceedings of the ASME 2012 Summer Heat Transfer Conference
HT2012
July 8-12, 2012, Rio Grande, Puerto Rico

HT2012-58222

NUMERICAL STUDY OF A SOLAR THERMOPHOTOVOLTAIC ENERGY CONVERTER WITH HIGH PERFORMANCE 2D PHOTONIC CRYSTALS

Youngsuk Nam[1,2], Yi Xiang Yeng[1], Peter Bermel[1], Marin Soljačić[1], and Evelyn N. Wang[1]

[1]Massachusetts Institute of Technology
Cambridge, MA, USA

[2]Kyung Hee University
Yongin, Korea

ABSTRACT

Solar thermophotovoltaic (STPV) systems convert solar energy into electricity via thermally radiated photons at tailored wavelength to increase energy conversion efficiency. In this work we report the design and analysis of a STPV using a high-fidelity 2D axisymmetric thermal-electrical hybrid model that includes thermal coupling between the absorber/emitter/PV cell and accounts for non-idealities such as temperature gradients and parasitic thermal losses. The radiative spectra of the absorber and emitter are engineered by using two-dimensional periodic square array of cylindrical holes on a tantalum (Ta) substrate. The optimal solar concentration and resulting temperature are determined by considering the energy losses associated with re-emission at the absorber, low energy (below band gap) emission at the emitter, and carrier thermalization /recombination in the PV cell. The modeling results suggest that the overall efficiency of a realistic planar STPV consisting of Ta PhCs and existing InGaAsSb PV cells with a filter can be as high as ~8%. The use of high performance PhCs allows us to simplify the system layout and operate STPVs at a significantly lower optical concentration level and operating temperature compared with STPVs using metallic cavity receivers. This work shows the importance of photon engineering for the development of high efficiency STPVs and offers design guidelines for both the PhC absorber/emitter and the overall system.

INTRODUCTION

Solar thermophotovoltaic (STPV) systems use an intermediate module that absorbs the solar radiation, and re-radiates photons at high temperatures and tailored wavelengths toward a photovoltaic (PV) cell (Fig.1). By converting the solar radiation to a narrow-banded thermal emission matching the spectral response of the PV cell, STPVs have the potential to overcome the Schockley-Queisser limit for PVs (<~40%) [1, 2]. STPVs are also highly scalable for a wide range of power capacity, have no moving parts, and allow solar energy storage and the use of an alternative fuel to generate electricity.

Despite the significant potential, very few experimental results have reported the overall efficiency. Of the studies reported, the demonstrated values were quite low due to the poor performance of the emitter/absorber/cell and the lack of understanding of the highly coupled energy transport processes among the components. A previous study using an eutectic emitter reported an extremely low (~0.025%) efficiency [3] and a recent experiment with a cylindrical tungsten thermal cavity and Ge cells demonstrated ~0.7% overall efficiency [4]. With a similar cylindrical layout, ~1% efficiency was achieved with a tantalum absorber/emitter and GaSb cells [5].

Recently, the use of photonic crystals (PhCs) with 1D periodic metal/dielectric layers or 2D array of cylindrical holes have been suggested to achieve a narrow-banded thermal emission with a tailored cut-off wavelength [6-8]. Long wavelength reflection filters also have been developed to reflect low energy emission back to the emitter [9, 10]. These previous studies, however, have focused on the component level performance rather than the system, which made it difficult to properly estimate overall performance of STPVs with these components. In STPVs, the spectral performance of absorber/emitter and the parasitic system-level thermal losses are strongly affected by operating temperature determined from the complex energy transport among the components (see Fig.1).

In this work, we developed a high-fidelity 2D axisymmetric thermal-electrical hybrid system-level model for STPVs with 2D Ta PhC absorbers/emitters. Our model includes radiative and conductive thermal coupling between the absorber/emitter/PV cell, and precisely accounts for non-idealities such as temperature gradients and parasitic thermal losses via the side wall (t) and gap (g) (Fig.1). The desired spectra are achieved by adjusting the cavity resonant frequency through changes in the micro-cavity dimensions and by matching the quality factor. Unlike previous studies [6, 8] the

angular dependence of PhCs are included in the system-level analysis and the PhCs are designed through the optimization process. By incorporating Ta PhC absorber/emitter, we show that ~8% overall efficiencies (without including a collector loss) can be achieved with the developed PhCs and existing cells/filters at a relatively low solar concentration (~100 Suns). The predicted efficiency is substantially higher than previously demonstrated values and our design has a much simpler layout than the previous STPVs with a cylindrical metal cavity.

MODEL FORMULATION

The simplified schematic of a planar STPV is shown in Figure 1. The concentrated solar energy is converted into heat at the absorber and reemitted through the emitter that is thermally coupled to the absorber. The thermally radiated high energy photons create electron-hole pairs and generate electricity while low energy photons are wasted as heat. The photons reflected on the PV cell surface or emitted from the cell are reabsorbed on the emitter.

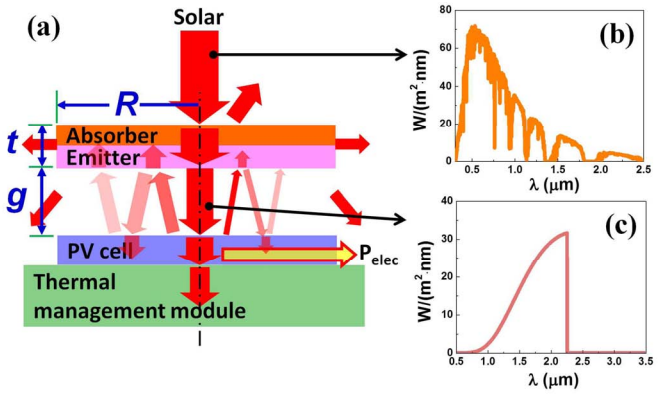

Figure 1: (a) Schematic of a planar STPV that converts wide spectrum solar radiation (b) into narrow-banded thermal emission (c). *R* and *t*: radius and thickness of a circular absorber/emitter module, g: gap between the emitter and cell.

We developed a hybrid model using the finite element method and an equivalent circuit model. The radiative heat transfer is coupled with conduction and convection heat transfer on each infinitesimal boundary element defined in a 2D or 3D framework (Eq.1):

$$-\vec{n}\cdot\left(-k\nabla T\right)=q_{rad}+h_{conv}(T_{\inf}-T) \quad on \;\; dA\,. \qquad (1)$$

On the absorber side (Eq.2), the radiative heat flux applied to each infinitesimal element (q_{rad} in Eq.1) is determined by incoming solar radiation and re-emission loss from the absorber:

$$q_{rad}=C_{opt}\cdot\int_0^\infty \alpha_a(\lambda)I_{solar}(\lambda)d\lambda-\int_0^\infty \varepsilon_a(\lambda)\{E_b(\lambda,T_a)-E_b(\lambda,T_{\inf})\}d\lambda\,. \qquad (2)$$

The standard solar spectrum for concentrated solar applications (AM1.5D) is used for the entire calculations. On the emitter side (Eq.3), the emission loss, re-absorption via multiple reflections between the emitter and the PV cell, and emission from the PV cell determine the radiative heat flux on each element (q_{rad} in Eq.1):

$$q_{rad}=-\int_0^\infty \varepsilon_e(\lambda)E_b(\lambda,T_e)d\lambda+\int_0^\infty \frac{\varepsilon_e(\lambda)^2E_b(\lambda,T_e)\rho_c(\lambda)F_{dA_e\to A_c}^{\;2}}{1-\rho_e(\lambda)\rho_c(\lambda)F_{dA_e\to A_c}^{\;2}}d\lambda \qquad (3)$$
$$+\int_0^\infty \frac{\varepsilon_e(\lambda)\varepsilon_c(\lambda)E_b(\lambda,T_c)F_{dA_e\to A_c}^{\;2}}{1-\rho_e(\lambda)\rho_c(\lambda)F_{dA_e\to A_c}^{\;2}}d\lambda$$

The temperature of PV cell is fixed at 300 K assuming the heat generated in the PV cell is dissipated via a thermal management module (see Fig.1). The view factor, $F_{dA\to Ac}$, quantifying the probability of a photon emitted by an infinitesimal element on emitter dA_e reaching a finite area of PV cell A_c can be calculated as:

$$F_{dA_e-A_c}=\int_{A_c}\frac{\cos\theta_e\cos\theta_c}{\pi S^2}dA_c\,, \qquad (4)$$

where θ_e and θ_c are the angles between the surface normal vectors and the line connecting dA_e and dA_c of length S. Since the absorber/emitter module has a finite thickness, a parasitic radiative loss through the side wall with emittance ε_s is defined as:

$$q_{rad}=-\int_0^\infty \varepsilon_s(\lambda)\{E_b(\lambda,T\,)-E_b(\lambda,T_{\inf})\}d\lambda\,. \qquad (5)$$

By substituting Eqs.2~5 into Eq.1, the overall energy balance and resulting temperature distributions are calculated, and then the total photocurrent generated in the PV cell is calculated from:

$$I_{ph}=\int_{A_e}\int_0^{\lambda_g} eF_{dA\to A_c}\eta_{ext}(\lambda)\frac{\lambda}{hc}\frac{\varepsilon_e(\lambda)E_b(\lambda,T_e)}{1-\rho_e(\lambda)\rho_c(\lambda)F_{dA\to A_c}^{\;2}}d\lambda dA\,, \qquad (6)$$

where η_{ext} represents the external quantum efficiency of PV cell, λ_g the band gap wavelength. The re-absorption of photons due to the multiple photon reflections between the emitter and PV cell (see Fig.1) are considered in Eq.6. Then the IV characterization of the PV cell and the maximum electrical power output is predicted from the equivalent circuit model:

$$I=I_{ph}-I_0\left(\exp\left(\frac{e\left(V+I\,R_s\right)}{n_i\,k_BT_c}\right)-1\right)-\frac{V+I\,R_s}{R_{sh}} \qquad (7)$$
$$\left.\frac{\partial(IV)}{\partial V}\right|_{P\max}=0$$

For a realistic prediction, various optical and electrical cell performance parameters such as quantum efficiency (η), reflectance of cell front surface (ρ_c), saturation current (I_0), ideality (n_i), series (R_s) and shunt (R_{sh}) resistances are determined based on the previous experimental characterizations [11].

STPV WITH IDEAL CUTOFF ABSORBER AND EMITTER

The ultimate performance of STPVs is obtained from an ideal angular selective absorber and monochromatic emitter [2]. Realizing these surfaces, however, is challenging with current technology, therefore we focus on more realistic spectrally selective cutoff absorbers and emitters ($\varepsilon = 1$ at $\lambda \leq \lambda_{cut}$ and $\varepsilon = 0$ at $\lambda > \lambda_{cut}$). The cutoff wavelengths of the emitter ($\lambda_{cut\text{-}emit}$) and absorber ($\lambda_{cut\text{-}abs}$) are determined from the band gap of the PV cell and the balance between solar absorption and re-emission loss, respectively.

To determine the emitter cutoff wavelength $\lambda_{cut\text{-}emit}$, the maximum efficiency of planar STPVs with an ideal cutoff absorber/emitter and ideal PV cell is calculated with varying the band gap of the PV cell in Figure 2. In this calculation, the $\lambda_{cut\text{-}emit}$ is equal to the band gap of PV and the optimal $\lambda_{cut\text{-}abs}$ is calculated from the overall energy balance and the resulting operating temperature. Only radiative recombination is considered for the ideal PV cell [12].

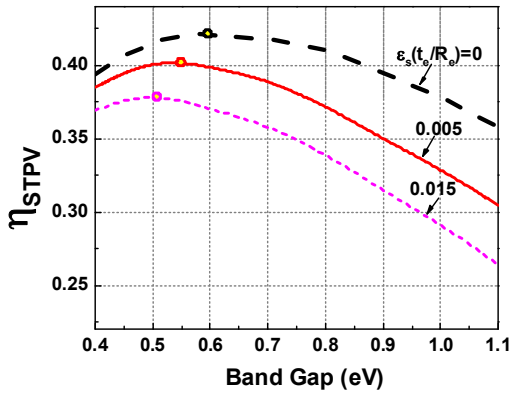

Figure 2: The predicted overall efficiency of planar STPVs with ideal cutoff absorbers/emitters and ideal PV cells. Dots show the optimal band gap for each effective side wall thickness.

The effects of parasitic radiative losses through the side wall (t in Fig.1) of the absorber/emitter module are also investigated by increasing the effective side wall thickness $\varepsilon_s(t/R)$ (ε_s is the emittance of side wall). Without any parasitic thermal loss through the sidewall $\varepsilon_s(t/R)=0$, the ideal band gap is located around 0.6 eV. When the parasitic loss is introduced, the optimal band gap decreases. The reduction of the band gap decreases the amount of energy emitted from the emitter, which increases the overall temperature of the absorber/emitter module at the same solar concentration. Due to the increase in temperature, the system with a large band gap becomes more sensitive to the parasitic thermal loss.

Based on the result, InGaAsSb PV cell (~0.55 eV) is selected for our STPV analysis. For a real system, we can limit the effective normalized side wall thickness at ~0.005 by using a thin absorber/emitter module with a low side wall emissivity (*e.g.*, $\varepsilon_s = 0.2$ and t/R=0.025).

Figure 3 shows the optimal absorber cutoff wavelength ($\lambda_{cut\text{-}abs}$) and resulting absorber efficiency (the ratio between the absorbed to arrived heat flux, Q_{abs}/H_{abs}). In general, the increase in solar concentration and decrease in absorber temperature provides higher efficiency due to the decrease in the relative re-emission loss. The optimal $\lambda_{cut\text{-}abs}$ and Q_{abs}/H_{abs} for the STPV with 0.55 eV are marked as an inset line in Figure 3.

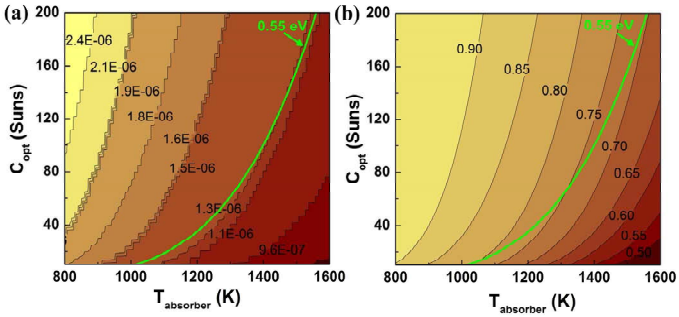

Figure 3: (a) The optimal cutoff wavelength and (b) the absorber efficiency for ideal spectrally selective cutoff absorbers. Inset line: the case when the cutoff wavelength of emitter is fixed at 2.25 μm to match the band gap of InGaAsSb PV cell (0.55 eV).

2D TANTALUM PHOTONIC CRYSTAL ABSORBER AND EMITTER

In order to realize the cutoff absorber and emitter applicable to high temperature systems, we engineered the radiative spectra of emitters and absorbers using a two-dimensional square array of cylindrical holes with period (a), radius (r), and depth (d) created on a tantalum (Ta) substrate (see the inset of Figure 4). This absorber and emitter exhibit near-blackbody emittance at short wavelengths as well as emittance almost as low as a polished metal at long wavelengths, with a sharp cutoff separating the two regimes. The cutoff wavelength is easily tunable by adjusting the fundamental cavity resonant frequency through changes in the cavities' dimensions, while maximum emittance below the cutoff is achieved via Q-matching [7, 13].

We utilized the mode matching formalism where the reflectance is calculated by matching the radiation fields at the boundary of free space and the cylindrical cavities via expansion of the cavity modes [14]. The dispersion of Ta was captured using the Lorentz-Drude model, fit both to measured

room temperature reflectance and elevated temperatures [15]. Overall, the normal and hemispherically averaged radiative properties are extremely close to the values obtained from the exact FDTD implementation [16]. The optimization is performed using both the Controlled Random Search algorithm [17] and the multi-level single-linkage (MLSL) algorithm using a low discrepancy sequence (LDS) [18]. The optimization is based on a figure of merit (FOM) measuring how close the performance is compared to an ideal cutoff emitter ($\varepsilon = 1$ at $\lambda \leq \lambda_{cut}$ and $\varepsilon = 0$ at $\lambda > \lambda_{cut}$).

$$FOM = 0.75\overline{E}_{\lambda \leq \lambda_{cut}} + 0.25(1 - \overline{E}_{\lambda > \lambda_{cut}}), \quad (8)$$

where $\overline{E}_{\lambda \leq \lambda_{cut}}$ and $\overline{E}_{\lambda > \lambda_{cut}}$ represent the average emittance above and below band gap, respectively. Figure 4 shows the resulting optimized radiative spectra of Ta PhCs. The cutoff wavelengths of the emitter and absorber are tailored to ~2.3 μm and ~1.3 μm, which takes into account the band gap of InGaAsSb PV cell (0.55 eV) and the balance between the solar absorption and the re-emission loss, respectively. Both normal (N) and hemispherically averaged (H) emittance are calculated.

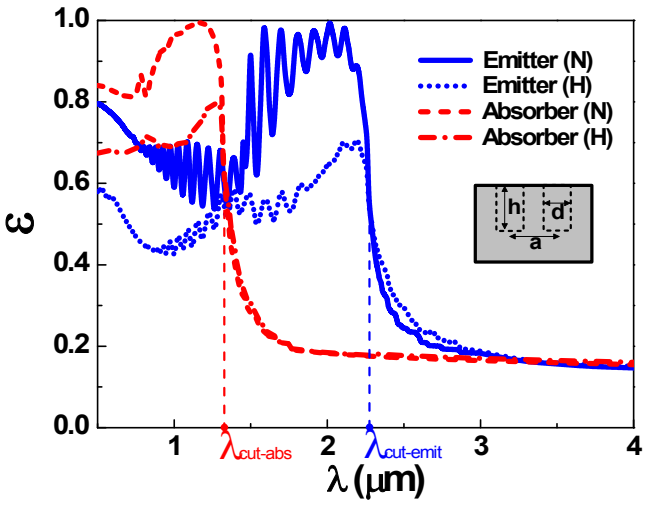

Figure 4: Simulated normal (N) and hemispherical (H) emittance for a developed PhC emitter ($\lambda_{cut\text{-}emit}$ = ~2.3 μm, a / d / h (μm) = 1.24 / 1.45 / 8.00) and absorber ($\lambda_{cut\text{-}abs}$ = ~1.3 μm, a / d / h (μm) = 0.68 / 0.78 / 7.94) designs, at 1200K.

RESULTS & DISCUSSION

EFFICIENCY BREAKDOWN

To elucidate the complex energy transport mechanism in STPVs, the overall efficiency is separated into the component level:

$$\eta_{STPV} = \frac{Q_{abs}}{H_{abs}} \cdot \frac{|Q_{emit}|}{Q_{abs}} \cdot \frac{Q_{emit,(E \geq E_g)}}{Q_{emit}} \cdot \frac{Q_{cell,(E \geq E_g)}}{|Q_{emit,(E \geq E_g)}|} \cdot \frac{P_{elec,\max}}{Q_{cell,(E \geq E_g)}}, \quad (8)$$
$$= \eta_{absorber} \cdot \eta_{adiabatic} \cdot \eta_{spectral} \cdot \eta_{cavity} \cdot \eta_{cell}$$

where Q and E_g represent net heat flux on each component surface and a band gap of PV cell, respectively.

Some portion of the incoming solar radiation is lost on the absorber due to the re-emission loss ($\eta_{absorber}$). The absorbed heat cannot be fully transferred to the emitter due to the parasitic thermal loss through the side wall ($\eta_{adiabatic}$). Among the total net thermal emission from the emitter, only high energy ($E \geq E_g$) photons can generate the electron-hole pair in the PV cell ($\eta_{spectral}$). Some amount of the useful emission is still lost due to the gap between the emitter and PV cell (η_{cavity}). Finally, the electron-hole recombination, thermalization, and non-ideal optical/electrical performance of the PV cell limit the conversion efficiency (η_{cell}).

STPVS WITH PHOTONIC CRYSTAL ABSORBER/ EMITTER

The optimized radiative properties of Ta PhCs are incorporated to the developed model. Co-axial circular absorber/emitter/PV cell of the same size are incorporated and the normalized thickness (t/R) and gap (g/R) were fixed at 0.05 for all cases. Solar concentration is limited to 200 Suns to maintain the operating temperature below ~1600 K. The analysis is performed with both ideal and existing InGaAsSb PV cells grown at MIT Lincoln lab. The non-idealities of the cell were experimentally characterized in the previous study [11] (η_{ext}=0.82, η_{int}=0.9, R_s=29.9×10^{-3} Ω, R_{sh}=204 Ω, I_0=10.8 μA, n=1.123).

In Figure 5, the performance obtained with PhC absorber/ emitter is compared with that with the ideal cutoff absorber/emitter (*Case I* vs. *II*). The effect of non-idealities of the PV cell on the overall performance is also quantified (*Case II* vs. *III*). The hemispherically averaged radiative properties (labeled as 'H' in Figure 4) are incorporated for a realistic prediction.

Compared with the ideal cutoff emitter (*Case I*), the PhC emitter (*Case II*) decreases the spectral efficiency by ~40% due to the low energy emission through the offset beyond $\lambda_{cut,emit}$. The PhC absorber (*Case II*) also reduces the absorber efficiency by ~40% due to the increase in re-emission loss through the offset beyond $\lambda_{cut,abs}$. Compared with the ideal PV cell, the implementation of the existing InGaAsSb PV cell drops the cell efficiency by ~50%. Due to the small normalized thickness (t/R) and gap (g/R), the adiabatic ($\eta_{adiabatic}$) and cavity (η_{cavity}) efficiencies are maintained around 95% in all cases. With the optimized Ta PhC absorber/emitter and existing InGaAsSb PV cell, overall STPV efficiency is predicted to be approximately 6.5% with ~100 suns of solar concentration (Fig.5a).

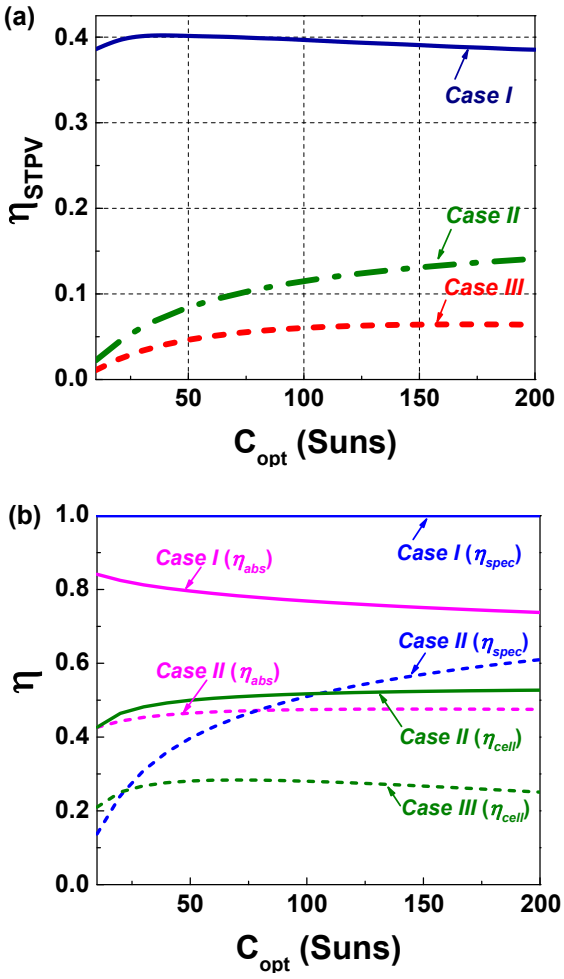

Figure 5: Overall STPV (a) and component level (b) efficiencies for *Case I~III*. The η_{abs}, η_{spec}, η_{cell} and η_{STPV} are defined in Equation 8. Solar concentration is limited to 200 Suns to maintain the operating temperature below ~1600K.
Case I: ideal cutoff absorber/emitter and ideal PV cell (0.55 eV) *Case II*: Ta PhC absorber/emitter and ideal PV cell (0.55 eV) *Case III*: Ta PhC absorber/emitter and existing Lincoln cell.

THE EFFECT OF LONG WAVELENGTH REFLECTION FILTER

Even with the PhC emitter, a significant amount of low energy photons are emitted through the offset beyond $\lambda_{cut,emit}$ (see Fig.4). To improve the spectral efficiency, we investigated the effects of a long wavelength filter attached to the PV cell on the STPV efficiency (*Case III* vs. *IV*). The analysis is based on the existing tandem filter developed by Lockheed Martin [19]. Figure 6 shows that the tandem filter improves the spectral efficiency over 30% by reflecting the low energy emission back to the absorber/emitter module. However, the absorber efficiency decreases by ~10% since the temperature of absorber/emitter module increases due to the enhanced re-absorption. The overall efficiency is predicted to be as high as ~8%, which shows that the use of tandem front filter can improve the overall efficiency over 15%. A more detailed efficiency breakdown is provided in Figure 7. The optimal optical concentration is determined by the balance between the component level efficiencies. The increase in the optical concentration significantly increases the spectral efficiency as the portion of low energy emission decreases. The overall efficiency, however, is not very sensitive to the concentration over 70 Suns since the increase in the spectral efficiency is balanced by the decrease in the cell efficiency.

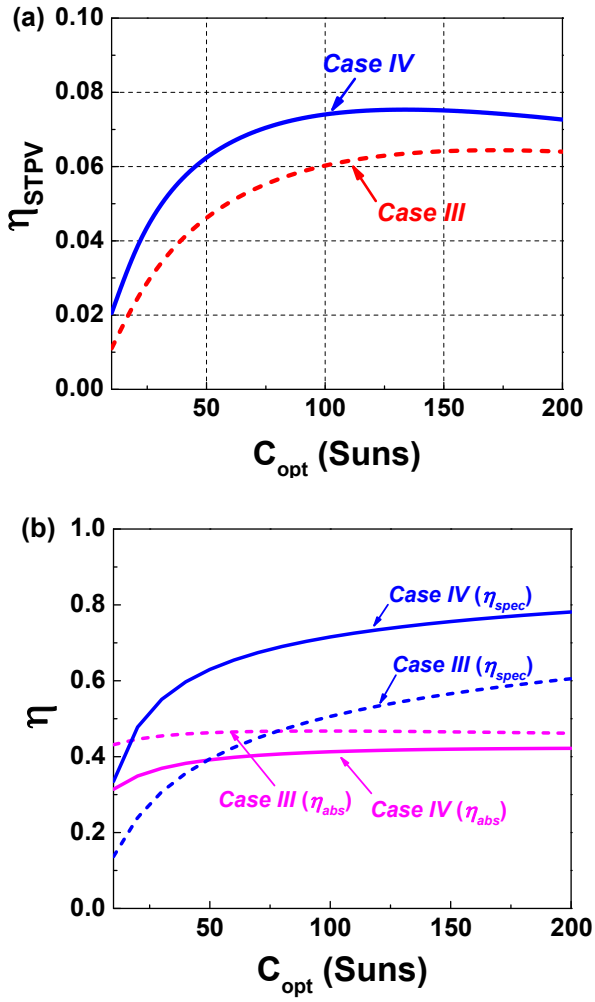

Figure 6: Overall STPV (a) and component level (b) efficiencies for *Case III* and *IV*. The η_{abs}, η_{spec}, and η_{STPV} are defined in Equation 8.
Case III: Ta PhC absorber/emitter and existing Lincoln cell
Case IV: Ta PhC absorber/emitter and existing Lincoln cell with a long wavelength reflection tandem filter.

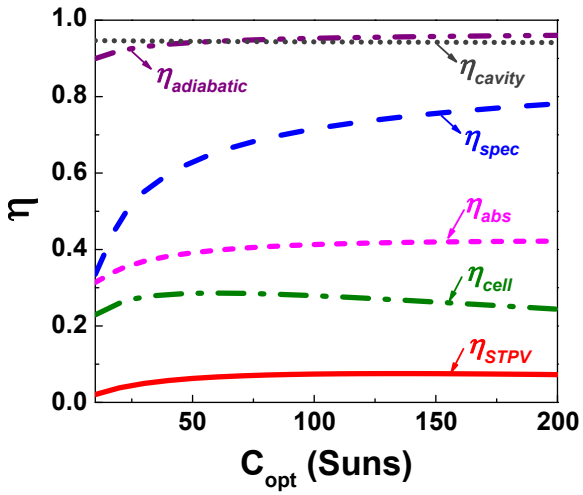

Figure 7: The efficiency breakdown as a function of solar concentration for a planar STPV composed of Ta PhCs and existing Lincoln cell with a tandem filter (*Case IV*).

CONCLUSIONS

We present the numerical analysis of a planar STPV composed of Ta photonic crystals and InGaAsSb PV cells. For a realistic prediction, we developed a high-fidelity 2D axisymmetric thermal-electrical hybrid system-level model including various non-idealities. The radiative spectra of PhCs are optimized by adjusting the cavity resonant frequency through changes in the cavity dimensions and by matching the quality factor. By incorporating the optimized 2D Ta PhC absorber/emitter and the existing PV cell with a long wavelength reflection filter, we show that the overall STPV efficiency can be as high as ~8% with a simple planar layout and low (~100 Suns) level of optical concentration. The efficiency can be further improved by enhancing the performance of PhCs and the quality of PV cells. The modeling approach discussed here will help develop high performance PhC absorbers/emitters and STPV systems.

NOMENCLATURE

A	Area [m^2]
c	Speed of light (in vaccum) [m/s]
C	Solar concentration [Sun]
E	Elementary charge = 1.602×10^{-19} [C]
E	Energy [J]
$\overline{E}$	Averaged Emissive power [W/m^2]
E_b	Blackbody Emissive power [W/m^2]
E_g	Band gap of PV cell [eV]
F	View factor [-]
g	Gap [m]
h	Heat transfer coefficient [W/m^2K], Planck's coefficient = 6.6261×10^{-34} [Js]
H	Irradiation on to surface [W/m^2]
I	Intensity of radiation [W/m^2 sr], current [A]
k	Thermal conductivity [W/mK]
k_B	Boltzmann's constant= 1.3807×10^{-23} [J/K]
n	Ideality [-]
q, Q	Net heat flux [W/m^2]
r, R	Resistance [Ω], radius [m]
t	Thickness [m]
T	Temperature [K]
P	Power [W/m^2]
V	Voltage [V]

Greek Symbols

α	Absorptance or absorptivity [-]
ε	Emittance or emissivity [-]
η	Efficiency [-]
λ	Wavelength [μm]
ρ	Reflectance or reflectivity [-]
ψ	Azimuthal angle [rad]

Subscript

a	Absorber
c	PV cell
cut	Cut-off
e	Emitter
elec	Electrical
ext	External
g	Band gap of PV cell
inf	Ambient
int	Internal
max	Maximum
opt	Optical
ph	Photocurrent
rad	Radiative
s	Series, sidewall
sh	Shunt
0	Saturation
w	Wall
η	Efficiency [-]
λ	Wavelength [μm]
ρ	Reflectance or reflectivity [-]

ACKNOWLEDGMENTS

All the authors gratefully acknowledge the support from the MIT S3TEC Center and the Energy Frontier Research Center funded by the Department of Energy, Office of Basic Energy Science.

REFERENCES

[1] W. Shockley and H. J. Queisser, "Detailed Balance Limit of Efficiency of p-n Junction Solar Cells,"

Journal of Applied Physics, vol. 32, pp. 510-519, 1961.

[2] N.-P. Harder and P. Würfel, "Theoretical limits of thermophotovoltaic solar energy conversion," *Semiconductor Science and Technology,* vol. 18, p. S151, 2003.

[3] H. Yugami*, et al.*, "Solar thermophotovoltaic using $Al_2O_3/Er_3Al_5O_{12}$ eutectic composite selective emitter," in *Photovoltaic Specialists Conference, 2000. Conference Record of the Twenty-Eighth IEEE*, 2000, pp. 1214-1217.

[4] A. Datas, "Development of Solar Thermophotovoltaic Systems," PhD, Universidad Politécnica de Madrid, 2011.

[5] V. Khvostikov*, et al.*, "Thermophotovoltaic generators based on gallium antimonide," *Semiconductors,* vol. 44, pp. 255-262, 2010.

[6] I. Celanovic*, et al.*, "Two-dimensional tungsten photonic crystals as selective thermal emitters," *Applied Physics Letters,* vol. 92, pp. 193101-3, 2008.

[7] M. Ghebrebrhan*, et al.*, "Tailoring thermal emission via Q matching of photonic crystal resonances," *Physical Review A,* vol. 83, p. 033810, 2011.

[8] P. Bermel*, et al.*, "Design and global optimization of high-efficiency thermophotovoltaic systems," *Opt. Express,* vol. 18, pp. A314-A334, 2010.

[9] J. TD Rahmlow*, et al.*, "Development of Front Surface, Spectral Control Filters with Greater Temperature Stability for Thermophotovoltaic Energy Conversion," in *AIP Conf. Proc.*, 2007, p. 59.

[10] R. T. Kristensen*, et al.*, "Frequency selective surfaces as near-infrared electromagnetic filters for thermophotovoltaic spectral control," *Journal of Applied Physics,* vol. 95, pp. 4845-4851, 2004.

[11] W. Chan*, et al.*, "Modeling low-bandgap thermophotovoltaic diodes for high-efficiency portable power generators," *Solar Energy Materials and Solar Cells,* vol. 94, pp. 509-514, 2010.

[12] P. Baruch*, et al.*, "On some thermodynamic aspects of photovoltaic solar energy conversion," *Solar Energy Materials and Solar Cells,* vol. 36, pp. 201-222, 1995.

[13] Y. X. Yeng*, et al.*, "Enabling high-temperature nanophotonics for energy applications," *Proceedings of the National Academy of Sciences,* vol. 109, pp. 2280-2285, February 14, 2012 2012.

[14] J. Bravo-Abad*, et al.*, "Resonant Transmission of Light Through Finite Chains of Subwavelength Holes in a Metallic Film," *Physical Review Letters,* vol. 93, p. 227401, 2004.

[15] Y. S. Touloukian, DeWitt, D.P., *Thermal radiative properties: metallic elements and alloys* vol. 7.0: New York, IFI/Plenum, 1970.

[16] A. F. Oskooi*, et al.*, "Meep: A flexible free-software package for electromagnetic simulations by the FDTD method," *Computer Physics Communications,* vol. 181, pp. 687-702, 2010.

[17] W. L. Price, "Global optimization by controlled random search," *Journal of Optimization Theory and Applications,* vol. 40, pp. 333-348, 1983.

[18] S. Kucherenko and Y. Sytsko, "Application of Deterministic Low-Discrepancy Sequences in Global Optimization," *Computational Optimization and Applications,* vol. 30, pp. 297-318, 2005.

[19] E. Brown*, et al.*, "The Status of Thermophotovoltaic Energy Conversion Technology at Lockheed Martin Corporation," LM-04K068, 2004.